Special phase matching of second-harmonic generation in helical ferroelectric liquid crystal cells

Hajime Hoshi, Doo-Han Chung, Ken Ishikawa, and Hideo Takezoe
Department of Organic and Polymeric Materials, Tokyo Institute of Technology, O-okayama, Meguro-ku, Tokyo 152-8552, Japan
(Received 5 July 2000; revised manuscript received 27 November 2000; published 18 April 2001)

The helical structures in ferroelectric liquid crystals can be utilized to realize a special phase matching for second-harmonic generation (SHG) when two counter fundamental waves propagate along the helical axis and the wavelength of SHG is near the photonic (selective reflection) band edge. On the basis of the exact theory [Drevensek-Olenik and Copic, Phys. Rev. E **56**, 581 (1997)], a simple analytical description is derived and some characteristic features of the special phase matching are shown. (1) Special phase matching is definitely achieved under particular combinations of polarization. (2) The SH spectrum is related to a subsidiary oscillating structure in the selective reflection spectrum. The maximum SH intensity is realized at the first dip of the oscillation near one of the edges in the selective reflection band. (3) The thickness (d) dependence of the maximum SH intensity is d^4 in thick cells, while it is d^2 for conventional phase matching. (4) The linewidth for the SH peak is d^{-3} dependent, which is much narrower than in conventional phase matching.

DOI: 10.1103/PhysRevE.63.056610 PACS number(s): 42.65.Ky, 42.70.Qs, 42.70.Df, 77.84.Nh

I. INTRODUCTION

Considerable attention has been paid to periodic dielectric media since the idea of the photonic band gap was discussed [1]. Phenomena occurring in photonic crystals are attractive from the viewpoints of both basic physics and device applications. The interest has been mostly devoted to two- and three-dimensional systems. This is partly because the aim of investigations of the photonic effect at first was to confine light in photonic crystals. However, the characteristic effect occurs not only in the photonic gap but also near the gap, where abnormal light propagation occurs because of strong dispersion of light. In this respect, one-dimensional photonic crystals also provide us with interesting phenomena, if light propagation, which is strongly influenced by the one-dimensional dielectric periodicity, is dealt with. One of these optical phenomena is optical harmonic generation. Because of the coherence of light, generated higher harmonic waves propagate along a certain direction, so that one can tune the direction of light propagation to obtain a strong influence of the photonic effect. Scalora *et al.* [2] and Haus *et al.* [3] theoretically studied the enhanced second-harmonic generation (SHG) in one-dimensional periodic structures.

We should emphasize here that some kinds of liquid crystal (LC) spontaneously form periodic (helical) structures, which provide more possibilities of realizing phase matching conditions than do homogeneous materials. Therefore, LCs themselves serve as ideal one-dimensional systems for studying the photonic effect. The difference that should be borne in mind is the variation in dielectric constants, namely, the dielectric constant varies sinusoidally along the helical axis, leading to (1) only one photonic gap without higher order ones, (2) optical eigenmodes with nearly circularly polarized light, and (3) a relatively wide gap due to the large dielectric anisotropy. The characteristic (1) is true only for light propagating along the helical axis and higher order stop bands appear for obliquely propagating waves.

Shelton and Shen showed many phase matchings for third-harmonic generation in cholesteric LCs [4–6]. For SHG, an additional phase matching, *special* phase matching, is possible under relatively general conditions without using color dispersion [7,8]. In the smectic-C^* (Sm-C^*) phase of ferroelectric LCs, this special phase matching is possible when two counterwaves propagate along the helical axis and the wavelength of SHG is near the selective reflection edge [9,10]. Although different conditions such as oblique incidence have been considered theoretically recently [11], only the above condition is dealt with in the present paper because of its simplicity. Special phase matching is superior to the conventional one in its thickness (d) dependence. The SH intensity is d^4 dependent for the special phase matching, while it is d^2 dependent for the conventional one. Because of this merit, special phase matching has received much attention.

Enhanced SHG under such conditions was observed by Kajikawa *et al.* [12] and by Furukawa *et al.* [13] using the Sm-C^* phases of MHPOOCBC and ROLIC6304, respectively. To explain these results, Copic and Drevensek-Olenik presented an analytical theory for the special phase matching in Sm-C^* phases and suggested that two counterwaves would be preferable to the unidirectional wave used in these experiments [9]. Yoo *et al.* confirmed the theoretical predictions using two counterwaves [10]. Recently, Drevensek-Olenik and Copic developed an exact theory, which computes the exact electromagnetic fields via a numerical method under the assumption that the power depletion of the fundamental waves is neglected [14]. This theory is consistent with recent polarization and thickness dependence experiments [15–17]. Although accurate results are obtained by the exact theory, it is difficult to grasp its general features because of the complicated numerical procedure. For example, the thickness dependence, which is expected to be special, has not been quantitatively analyzed. To help in understanding, the electric fields in LCs were visualized in a previous paper and some features were noted [18]. In the present paper, a simple analysis is developed based on the exact theory. The effect of polarization is explicitly considered, which is rather undetermined in the previous analytical method by Copic and Drevensek-Olenik [9]. The phase matching conditions are definitely determined. Unusual

thickness dependence and linewidth properties are also discussed.

II. EXACT THEORY

Analytical expressions are derived based on the exact theory [14]. To define the notations, the exact theory is briefly reviewed in this section. In this model, three (left, middle, right) layers are considered. The left and right layers are isotropic substrates (dielectric constants ε_l and ε_r at the fundamental frequency ω and ε_L and ε_R at 2ω, respectively). The middle layer (thickness d) consists of a Sm-C^* structure with local C_2 symmetry, the axis of which forms a helical structure (pitch p) with the helical axis normal to the substrate surface. Local Cartesian coordinates (e_1,e_2,e_3) are introduced, where the e_2 and e_3 axes are parallel to the C_2 axis and the major principal axis of the dielectric constant (molecular long axis), respectively. In these coordinates, the nonzero components of the dielectric constant and the nonlinear optical susceptibility are ε_{11}, ε_{22}, and ε_{33} (or simply ε_1, ε_2, and ε_3) at ω, $\tilde{\varepsilon}_{11}$, $\tilde{\varepsilon}_{22}$, and $\tilde{\varepsilon}_{33}$ (or $\tilde{\varepsilon}_1$, $\tilde{\varepsilon}_2$, and $\tilde{\varepsilon}_3$) at 2ω, and χ_{123}, χ_{112}, χ_{332}, and χ_{222}, where Kleinman's symmetry is assumed for $\chi^{(2)}$. The tilt angle θ is the angle between the e_3 axis and the helical axis. In this analysis, depletion of the fundamental waves is neglected and only normally incident fundamental waves are treated. Laboratory coordinates xyz (e_x,e_y,e_z), are related to the local coordinates by

$$\begin{pmatrix} e_x \\ e_y \\ e_z \end{pmatrix} = R \begin{pmatrix} e_1 \\ e_2 \\ e_3 \end{pmatrix} = \begin{pmatrix} \cos\theta\cos qz & -\sin qz & \sin\theta\cos qz \\ \cos\theta\sin qz & \cos qz & \sin\theta\sin qz \\ -\sin\theta & 0 & \cos\theta \end{pmatrix} \times \begin{pmatrix} e_1 \\ e_2 \\ e_3 \end{pmatrix},$$

where z is the helical axis and $q=2\pi/p$, which is positive (negative) for a right- (left)-handed helix.

A. Propagation of fundamental waves: Homogeneous waves

The fundamental waves are described by the wave equation in a nonmagnetic system [14,19,20]

$$\nabla\times\nabla\times\mathbf{E}+\frac{\varepsilon}{c^2}\frac{\partial^2\mathbf{E}}{\partial t^2}=0.$$

For plane waves propagating along the z axis, the wave equation in xyz coordinates is

$$(-\partial_z^2 I_{ij}^0 - k_0^2\varepsilon'_{ij})E'_j=0, \quad I^0\equiv\begin{pmatrix} 1 & 0 & 0 \\ 0 & 1 & 0 \\ 0 & 0 & 0 \end{pmatrix}, \tag{1}$$

where time factor $e^{-i\omega t}$ of the electric field is eliminated, $k_0=\omega/c$, and ε'_{ij} and E'_j are the components in xyz coordinates. This equation is known to have a de Vries type solution [21,22] and is simplified using unitary transformed coordinates (e_a,e_b,e_z), where

$$\begin{pmatrix} e_a \\ e_b \\ e_z \end{pmatrix} = W \begin{pmatrix} e_x \\ e_y \\ e_z \end{pmatrix} = \frac{1}{\sqrt{2}} \begin{pmatrix} -e^{-iqz} & -ie^{-iqz} & 0 \\ e^{iqz} & -ie^{iqz} & 0 \\ 0 & 0 & \sqrt{2} \end{pmatrix} \begin{pmatrix} e_x \\ e_y \\ e_z \end{pmatrix}. \tag{2}$$

As discussed in Appendix A, the general homogeneous solutions are linear combinations of four waves. In abz coordinates, they are given by

$$\begin{pmatrix} E_a \\ E_b \\ E_z \end{pmatrix} = \begin{pmatrix} f_1 e^{ik_1 z} & f_2 e^{ik_2 z} & f_3 e^{ik_3 z} & f_4 e^{ik_4 z} \\ e^{ik_1 z} & e^{ik_2 z} & e^{ik_3 z} & e^{ik_4 z} \\ (1-f_1)e^{ik_1 z}\varepsilon_{az}/\varepsilon_{zz} & (1-f_2)e^{ik_2 z}\varepsilon_{az}/\varepsilon_{zz} & (1-f_3)e^{ik_3 z}\varepsilon_{az}/\varepsilon_{zz} & (1-f_4)e^{ik_4 z}\varepsilon_{az}/\varepsilon_{zz} \end{pmatrix} \mathbf{a}, \tag{3}$$

$$\mathbf{a}\equiv{}^t(a_1 a_2 a_3 a_4),$$

where

$$k_t=\pm(q^2+lk_0^2\pm\sqrt{4lk_0^2q^2+m^2k_0^4})^{1/2}, \tag{4}$$

$$f_t=\frac{E_a}{E_b}=\frac{(k_t-q)^2-lk_0^2}{mk_0^2}, \tag{5}$$

$$l\equiv\{\varepsilon_1+\varepsilon_2+(\varepsilon_3-\varepsilon_1)\varepsilon_1\sin^2\theta/(\varepsilon_1\sin^2\theta+\varepsilon_3\cos^2\theta)\}/2,$$

$$m\equiv -l+\varepsilon_2. \tag{6}$$

ε_{az} and ε_{zz} are given in Appendix A, and t (=1–4) specifies four modes defined by choosing two $\pm$ signs in Eq. (4). In xyz coordinates, E_x, E_y, H_x, and H_y components are given by

$$\begin{pmatrix} E_x \\ E_y \\ H_x \\ H_y \end{pmatrix} = \sum_{t=1}^{4} \frac{a_t}{\sqrt{2}} \begin{pmatrix} -f_t e^{i(k_t+q)z} + e^{i(k_t-q)z} \\ i\{f_t e^{i(k_t+q)z} + e^{i(k_t-q)z}\} \\ -\frac{i}{k_0}\{f_t(k_t+q)e^{i(k_t+q)z} + (k_t-q)e^{i(k_t-q)z}\} \\ \frac{1}{k_0}\{-f_t(k_t+q)e^{i(k_t+q)z} + (k_t-q)e^{i(k_t-q)z}\} \end{pmatrix} \equiv P(z)\mathbf{a}. \tag{7}$$

B. The boundary conditions for fundamental waves

The coefficients **a** are determined by the boundary conditions. Let E_{lx}^0 and E_{ly}^0 (E_{rx}^0 and E_{ry}^0) be the x and y components of the electric field amplitude that is incident on the left (right) side of the cell. Similarly, let F_{lx}^0 and F_{ly}^0 (F_{rx}^0 and F_{ry}^0) be the x and y components of the electric field amplitude that emanates from the left (right) side. E_x, E_y, H_x, and H_y components for the waves incident (I) and emanating (F) from the left and right sides are given by

$$I_l = \begin{pmatrix} E_{lx}^0 \\ E_{ly}^0 \\ -\sqrt{\varepsilon_l} E_{ly}^0 \\ \sqrt{\varepsilon_l} E_{lx}^0 \end{pmatrix}, \quad I_r = \begin{pmatrix} E_{rx}^0 \\ E_{ry}^0 \\ \sqrt{\varepsilon_r} E_{ry}^0 \\ -\sqrt{\varepsilon_r} E_{rx}^0 \end{pmatrix},$$

$$F_l = \begin{pmatrix} F_{lx}^0 \\ F_{ly}^0 \\ \sqrt{\varepsilon_l} F_{ly}^0 \\ -\sqrt{\varepsilon_l} F_{lx}^0 \end{pmatrix}, \quad F_r = \begin{pmatrix} F_{rx}^0 \\ F_{ry}^0 \\ -\sqrt{\varepsilon_r} F_{ry}^0 \\ \sqrt{\varepsilon_r} F_{rx}^0 \end{pmatrix}. \tag{8}$$

The boundary conditions are expressed as

$$I_l + F_l = P(0)\mathbf{a}.$$

$$I_r + F_r = P(d)\mathbf{a}.$$

Using the relations

$$F_l = S_l F, \quad F_r = S_r F,$$

where F, S_l, and S_r are defined as

$$F \equiv \begin{pmatrix} F_{lx}^0 \\ F_{ly}^0 \\ F_{rx}^0 \\ F_{ry}^0 \end{pmatrix}, \quad S_l \equiv \begin{pmatrix} 1 & 0 & 0 & 0 \\ 0 & 1 & 0 & 0 \\ 0 & \sqrt{\varepsilon_l} & 0 & 0 \\ -\sqrt{\varepsilon_l} & 0 & 0 & 0 \end{pmatrix},$$

$$S_r \equiv \begin{pmatrix} 0 & 0 & 1 & 0 \\ 0 & 0 & 0 & 1 \\ 0 & 0 & 0 & -\sqrt{\varepsilon_r} \\ 0 & 0 & \sqrt{\varepsilon_r} & 0 \end{pmatrix}, \tag{9}$$

the boundary conditions are expressed in 8×8 matrix form as

$$\begin{pmatrix} P(d) & -S_r \\ P(0) & -S_l \end{pmatrix} \begin{pmatrix} \mathbf{a} \\ F \end{pmatrix} = \begin{pmatrix} I_r \\ I_l \end{pmatrix}. \tag{10}$$

For exact numerical calculations, the Gauss elimination method was applied.

C. Propagation of SH waves: Inhomogeneous and homogeneous waves

The SH waves produced by nonlinear polarization **P** are described by

$$\nabla \times \nabla \times \mathbf{E} + \frac{\tilde{\varepsilon}}{c^2} \frac{\partial^2 \mathbf{E}}{\partial t^2} = -\frac{4\pi}{c^2} \frac{\partial^2 \mathbf{P}}{\partial t^2}. \tag{11}$$

The particular or inhomogeneous solution is obtained as follows (see Appendix B). In *abz* coordinates, **P** has the form

$$\begin{pmatrix} P_a \\ P_b \\ P_z \end{pmatrix} = \sum_{i,j=1}^{4} \begin{pmatrix} P_{aij}^0 \\ P_{bij}^0 \\ P_{zij}^0 \end{pmatrix} e^{ik_{ij}z}, \quad k_{ij} \equiv k_i + k_j, \tag{12}$$

and the inhomogeneous solution is given by

$$\begin{pmatrix} E_a \\ E_b \\ E_z \end{pmatrix} = \sum_{ij} \begin{pmatrix} E_{aij}^0 \\ E_{bij}^0 \\ E_{zij}^0 \end{pmatrix} e^{ik_{ij}z}, \tag{13}$$

where

$$\begin{pmatrix} E^0_{aij} \\ E^0_{bij} \\ E^0_{zij} \end{pmatrix} = \frac{-4\pi}{\Delta}$$

$$\times \begin{pmatrix} L-\dfrac{(k_{ij}-q)^2}{K_0^2} & -M & \dfrac{\tilde{\varepsilon}_{az}}{\tilde{\varepsilon}_{zz}}\left\{-\tilde{\varepsilon}_2+\dfrac{(k_{ij}-q)^2}{K_0^2}\right\} \\ -M & L-\dfrac{(k_{ij}+q)^2}{K_0^2} & \dfrac{\tilde{\varepsilon}_{az}}{\tilde{\varepsilon}_{zz}}\left\{\tilde{\varepsilon}_2-\dfrac{(k_{ij}+q)^2}{K_0^2}\right\} \\ \dfrac{\tilde{\varepsilon}_{az}}{\tilde{\varepsilon}_{zz}}\left\{-\tilde{\varepsilon}_2+\dfrac{(k_{ij}-q)^2}{K_0^2}\right\} & \dfrac{\tilde{\varepsilon}_{az}}{\tilde{\varepsilon}_{zz}}\left\{\tilde{\varepsilon}_2-\dfrac{(k_{ij}+q)^2}{K_0^2}\right\} & \dfrac{\tilde{\varepsilon}_2\{\tilde{\varepsilon}_1+\tilde{\varepsilon}_3+(\tilde{\varepsilon}_1-\tilde{\varepsilon}_3)\cos 2\theta\}}{2\tilde{\varepsilon}_{zz}}-\dfrac{2\tilde{\varepsilon}_{aa}(k_{ij}^2+q^2)}{\tilde{\varepsilon}_{zz}K_0^2}+\dfrac{(k_{ij}^2-q^2)^2}{\tilde{\varepsilon}_{zz}K_0^4} \end{pmatrix}$$

$$\times \begin{pmatrix} P^0_{aij} \\ P^0_{bij} \\ P^0_{zij} \end{pmatrix}, \tag{14}$$

$$\Delta = L^2-M^2-\frac{2L}{K_0^2}(k_{ij}^2+q^2)+\frac{(k_{ij}^2-q^2)^2}{K_0^4} = (k_{ij}-K_1)(k_{ij}-K_2)(k_{ij}-K_3)(k_{ij}-K_4)/K_0^4, \tag{15}$$

$K_0=2\omega/c$, and $\tilde{\varepsilon}_{\alpha\beta}$, L, M, and K_t are defined by Eqs. (A3), (6), and (4) using the dielectric constants at 2ω. In xyz coordinates, E_x, E_y, H_x, and H_y components for the inhomogeneous waves are given by

$$\begin{pmatrix} E_x \\ E_y \\ H_x \\ H_y \end{pmatrix} = \frac{1}{\sqrt{2}}\sum_{ij}\begin{pmatrix} -E^0_{aij}e^{i(k_{ij}+q)z}+E^0_{bij}e^{i(k_{ij}-q)z} \\ i\{E^0_{aij}e^{i(k_{ij}+q)z}+E^0_{bij}e^{i(k_{ij}-q)z}\} \\ -\dfrac{i}{K_0}\{E^0_{aij}(k_{ij}+q)e^{i(k_{ij}+q)z}+E^0_{bij}(k_{ij}-q)e^{i(k_{ij}-q)z}\} \\ \dfrac{1}{K_0}\{-E^0_{aij}(k_{ij}+q)e^{i(k_{ij}+q)z}+E^0_{bij}(k_{ij}-q)e^{i(k_{ij}-q)z}\} \end{pmatrix} \equiv u_p(z), \tag{16}$$

where the subscript p stands for particular (or inhomogeneous) solution.

On the other hand, E_x, E_y, H_x, and H_y components for the homogeneous waves are given by the same form as Eq. (7):

$$\begin{pmatrix} E_x \\ E_y \\ H_x \\ H_y \end{pmatrix} = \sum_{t=1}^{4}\frac{A_t}{\sqrt{2}}\begin{pmatrix} -F_te^{i(K_t+q)z}+e^{i(K_t-q)z} \\ i\{F_te^{i(K_t+q)z}+e^{i(K_t-q)z}\} \\ -\dfrac{i}{K_0}\{F_t(K_t+q)e^{i(K_t+q)z}+(K_t-q)e^{i(K_t-q)z}\} \\ \dfrac{1}{K_0}\{-F_t(K_t+q)e^{i(K_t+q)z}+(K_t-q)e^{i(K_t-q)z}\} \end{pmatrix} \equiv \Pi(z)\mathbf{A}, \tag{17}$$

where F_t is defined by Eq. (5) using the dielectric constants at 2ω.

D. The boundary conditions for SH waves

The waves emanating from the cell and **A** are determined by the boundary conditions. Let F^0_{Lx} and F^0_{Ly} (F^0_{Rx} and F^0_{Ry}) be the x and y components of the SH electric field amplitude that emanates from the left (right) side. E_x, E_y, H_x, and H_y components for these waves are given by

$$F_L=\begin{pmatrix} F^0_{Lx} \\ F^0_{Ly} \\ \sqrt{\varepsilon_L}F^0_{Ly} \\ -\sqrt{\varepsilon_L}F^0_{Lx} \end{pmatrix}, \quad F_R=\begin{pmatrix} F^0_{Rx} \\ F^0_{Ry} \\ -\sqrt{\varepsilon_R}F^0_{Ry} \\ \sqrt{\varepsilon_R}F^0_{Rx} \end{pmatrix}. \tag{18}$$

The boundary conditions are

$$\begin{aligned} F_L &= u_p(0)+\Pi(0)\mathbf{A}. \\ F_R &= u_p(d)+\Pi(d)\mathbf{A}. \end{aligned} \tag{19}$$

Using the definitions

$$\mathcal{F}\equiv=\begin{pmatrix} F^0_{Lx} \\ F^0_{Ly} \\ F^0_{Rx} \\ F^0_{Ry} \end{pmatrix}, \quad S_L\equiv\begin{pmatrix} 1 & 0 & 0 & 0 \\ 0 & 1 & 0 & 0 \\ 0 & \sqrt{\varepsilon_L} & 0 & 0 \\ -\sqrt{\varepsilon_L} & 0 & 0 & 0 \end{pmatrix},$$

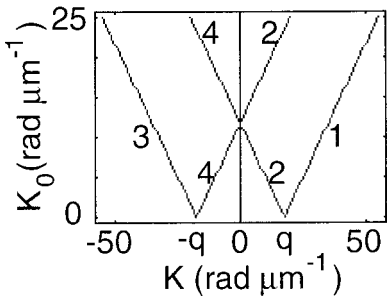

FIG. 1. Dispersion curves for propagation along the helical axis in Sm-C^*. Four modes are defined by Eq. (22).

$$S_R \equiv \begin{pmatrix} 0 & 0 & 1 & 0 \\ 0 & 0 & 0 & 1 \\ 0 & 0 & 0 & -\sqrt{\varepsilon_R} \\ 0 & 0 & \sqrt{\varepsilon_R} & 0 \end{pmatrix}, \tag{20}$$

the boundary conditions are expressed in 8×8 matrix form as

$$\begin{pmatrix} \Pi(d) & -S_R \\ \Pi(0) & -S_L \end{pmatrix} \begin{pmatrix} \mathbf{A} \\ \mathcal{F} \end{pmatrix} = \begin{pmatrix} -u_p(d) \\ -u_p(0) \end{pmatrix}, \tag{21}$$

and solved by the Gauss elimination method.

III. ANALYSIS AND DISCUSSION

The special phase matching is analyzed based on the exact theory. In previous papers, the exact theory was found to be consistent with experimental results [15–17]. However, the general features have not been described yet. Most of the experiments were performed using a Nd:YAG (yttrium aluminum garnet) laser as the fundamental wave (wavelength 1.064 μm) and ROLIC6304 [10,13,15–17]. In the present paper, the numerical results are obtained under these conditions. The molecules form a right-handed helix whose axis is normal to the glass substrate. The dielectric constants of ROLIC6304 and glass are $\varepsilon_1=\tilde{\varepsilon}_1=\varepsilon_2=\tilde{\varepsilon}_2=2.2$, $\varepsilon_3=\tilde{\varepsilon}_3=2.8$, $\varepsilon_1=\varepsilon_L=\varepsilon_r=\varepsilon_R=2.25$ [17,23]. The tilt angle θ is 23° [17,23]. $\chi^{(2)}$ components are $\chi_{123}:\chi_{112}:\chi_{332}:\chi_{222}=0.34:-1.12:-2.76:3.34$, determined by standard angle phase matching using the unwound sample under an electric field [23]. In the previous experiments, the pitch was tuned by the temperature. Special phase matching was actually observed when the selective reflection band was located near 0.532 μm [10,13,15–17].

A. Dispersion relations and homogeneous wave modes

First let us consider the homogeneous waves [Eqs. (7) and (17)] in LCs, which are responsible for the linear optical properties [19,20]. We use Eq. (17), namely, ε at 2ω, because the results are applied to SH waves in the following section. Figure 1 shows the dispersion curves [9,14] using $p=0.358\,761\,84\,\mu$m ($q=17.513\,527$ rad μm^{-1}), where the four modes of K are defined as follows:

$$\begin{aligned} K_1 &= +(q^2+LK_0^2+\sqrt{4LK_0^2q^2+M^2K_0^4})^{1/2}, \\ K_2 &= +(q^2+LK_0^2-\sqrt{4LK_0^2q^2+M^2K_0^4})^{1/2}, \\ K_3 &= -K_1, \\ K_4 &= -K_2. \end{aligned} \tag{22}$$

K_2 and K_4 are imaginary when K_0 is between $K_{02}\equiv q/\sqrt{L+M}$ and $K_{013}\equiv q/\sqrt{L-M}$, namely, the wavelength in vacuo, $\lambda_0(2\omega)$, is between $\lambda_2\equiv\sqrt{L+M}p$ and $\lambda_{13}\equiv\sqrt{L-M}p$, which correspond to the edges of the photonic gap in Fig. 1. Using the relations

$$L+M=\tilde{\varepsilon}_2, \quad L-M=\tilde{\varepsilon}_e\equiv\tilde{\varepsilon}_1\tilde{\varepsilon}_3/(\tilde{\varepsilon}_1\sin^2\theta+\tilde{\varepsilon}_3\cos^2\theta), \tag{23}$$

the λ_2 (K_{02}) edge is determined by $\tilde{\varepsilon}_2$ and the λ_{13} (K_{013}) edge is determined by $\tilde{\varepsilon}_1$, $\tilde{\varepsilon}_3$, and θ. For ROLIC6304, K_{02} is higher than K_{013} because of the negative M. In previous papers, $L\equiv\tilde{\varepsilon}$ is defined as the average value of the dielectric tensor, whereas $-M\equiv\alpha$ is defined as the dielectric anisotropy in the plane of the smectic layer [9,14]. These definitions are obvious in the following form:

$$L=(\tilde{\varepsilon}_2+\tilde{\varepsilon}_e)/2, \quad M=(\tilde{\varepsilon}_2-\tilde{\varepsilon}_e)/2. \tag{24}$$

L and $|M|$ are important factors for determining the location and the width of the gap, respectively. Actually we note that $|\lambda_2-\lambda_{13}|$ is proportional to the optical anisotropy of the refractive index in the plane of the smectic layer, $|\sqrt{\tilde{\varepsilon}_2}-\sqrt{\tilde{\varepsilon}_e}|$.

To characterize the modes, we concentrate on the following part of the homogeneous wave:

$$\begin{pmatrix} E_x \\ E_y \end{pmatrix} = \sum_{t=1}^{4} \frac{A_t}{\sqrt{2}} \left\{ \begin{pmatrix} -F_t e^{i(K_t+q)z} \\ iF_t e^{i(K_t+q)z} \end{pmatrix} + \begin{pmatrix} e^{i(K_t-q)z} \\ ie^{i(K_t-q)z} \end{pmatrix} \right\}. \tag{25}$$

The first and second terms express either l or r components. The signs of K_t+q and K_t-q define the propagation directions of the first and second terms, respectively. Positive and negative values of K_t+q correspond to propagation of r polarization toward the $+z$ direction, $(+z,r)$, and propagation of l polarization toward the $-z$ direction, $(-z,l)$, respectively. Those of K_t-q correspond to $(+z,l)$, and $(-z,r)$, respectively. The ratio of the first and second terms is F_t:1 and $|F_1|$ and $|F_2|$ are shown in Fig. 2. Using Eqs. (A7) and (5), F_3 and F_4 are related to F_1 and F_2 by

$$F_1F_3=F_2F_4=1. \tag{26}$$

Using Eq. (25) and Figs. 1 and 2, four modes can be characterized. For mode 1, $|F_1|\ll 1$ as shown in Fig. 2, which indicates that the second term is dominant. Moreover, K_1-q is positive as shown in Fig. 1. Thus, mode 1 is dominated by $(+z,l)$. Similarly, mode 3 is dominated by $(-z,l)$.

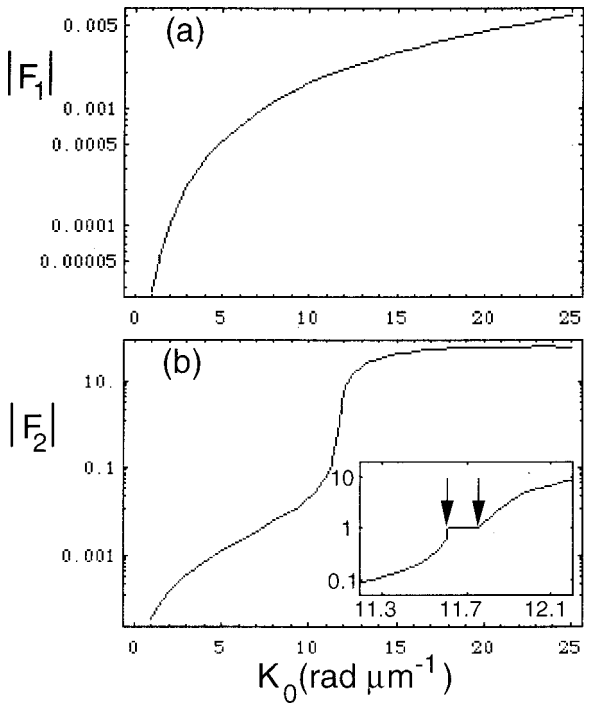

FIG. 2. (a) $|F_1|$ and (b) $|F_2|$ versus K_0 using Eq. (5). The inset shows the region near the photonic band gap. The arrows indicate the edges of the band.

Modes 2 and 4 are considered separately for the three region (I) inside the gap, (II) far from the gap, and (III) outside the gap and close to the edge.

In region I marked by the arrows in Fig. 2, K_2 and K_4 are purely imaginary,

$$K_2 = is, \quad K_4 = -is, \tag{27}$$

where s is a real function. Modes 2 and 4 are exponentially growing and decreasing waves. So the selective reflection occurs when a wave whose helicity is the same as that of the helix is incident. Since the complex conjugate of F_2, $\overline{F_2}$, satisfies the relation, $\overline{F_2} = F_4 = 1/F_2$, F_2 and F_4 are expressed as

$$F_2 = e^{i\phi}, \quad F_4 = e^{-i\phi}, \tag{28}$$

where ϕ is a real function. In particular, $|F_2| = 1$ in this region as shown in Fig. 2.

In region II, $|F_2| \ll 1$ is satisfied below the gap, and $|F_2| \gg 1$ is satisfied above the gap, which indicates that modes 2 and 4 are dominated by the r polarized wave. For mode 2, $(-z,r)$ is dominant below the gap and $(+z,r)$ is dominant above the gap. For mode 4,$(+z,r)$ is dominant below the gap and $(-z,r)$ is dominant above the gap.

In region III, the simple interpretation for region II is not applicable since $|F_2|$ is close to 1 and two terms in Eq. (25) should be considered. Near the edges, both modes 2 and 4 are linear combinations of $(+z,r)$ and $(-z,r)$. In particular, at the λ_2 edge, $F_2 = 1$, and Eq. (17) is expressed as

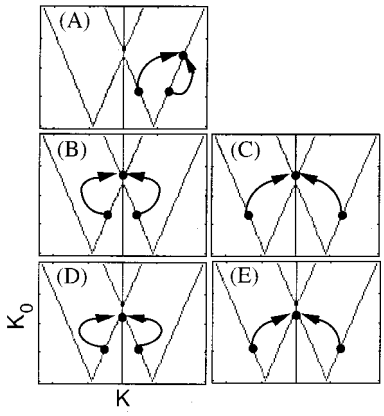

FIG. 3. Possible phase matching conditions when SH frequency is located near the photonic band gap.

$$A_2 \Pi(z)_2 = \begin{pmatrix} E_x \\ E_y \\ H_x \\ H_y \end{pmatrix} = \sqrt{2} \begin{pmatrix} -i \sin qz \\ i \cos qz \\ (q \sin qz)/K_0 \\ -(q \cos qz)/K_0 \end{pmatrix} A_2, \tag{29}$$

$E_z = H_z = 0$, which is a standing wave in right-handed helical form whose electric and magnetic fields are always parallel to the C_2 axis. On the other hand, at the λ_{13} edge, $F_2 = -1$, and Eq. (17) is expressed as

$$A_2 \Pi(z)_2 = \sqrt{2} \begin{pmatrix} \cos qz \\ \sin qz \\ (iq \cos qz)/K_0 \\ (iq \sin qz)/K_0 \end{pmatrix} A_2, \tag{30}$$

$E_z = 2A_2 \tilde{\varepsilon}_{az}/\tilde{\varepsilon}_{zz}$, $H_z = 0$, which is a standing wave in right-handed helical form whose electric and magnetic fields are always normal to the C_2 axis. In other words, this wave is orthogonal to the wave at the λ_2 edge.

B. Second-harmonic generation

1. Phase matching conditions

Let us consider SHG properties. Enhanced SHG is expected when the amplitudes of the inhomogeneous waves are large. According to Eq. (15), this situation occurs under phase matching conditions, namely,

$$k_{ij} \equiv k_i + k_j = K_t. \tag{31}$$

Under the condition that the SH frequency is located near the photonic band gap, possible conditions $A-E$ are illustrated in Fig. 3 using the diagrams of Drevensek-Olenik and Copic [14]. It is clear that no color dispersion is necessary and umklapp processes are involved.

Phase matching A occurs when $k_{12} \equiv k_1 + k_2 = K_1$. To realize this phase matching, two counter fundamental waves, one with $(+z,l)$ and the other with $(-z,r)$, $(+z,l;-z,r)$, are effective.

Phase matchings $B-E$ occur when $K_0 = K_{02}$ or $K_0 = K_{013}$. For phase matchings B and D, counterwaves with r

polarization $(+z,r;-z,r)$ are effective, while, for C and E, counterwaves with l polarization $(+z,l;-z,l)$, are effective.

2. Type-II-like phase matching A

The condition for phase matching A is $k_{12}=K_1$ and the effective fundamental waves are $(+z,l;-z,r)$, whose polarizations differ from each other (type II like). SHG under such conditions is analyzed. In *abz* coordinates, the homogeneous fundamental waves [Eq. (3)] are dominated by

$$\begin{pmatrix} E_a \\ E_b \\ E_z \end{pmatrix} \simeq \begin{pmatrix} 0 \\ a_1 e^{ik_1 z} + a_2 e^{ik_2 z} \\ (a_1 e^{ik_1 z} + a_2 e^{ik_2 z})\varepsilon_{az}/\varepsilon_{zz} \end{pmatrix}. \tag{32}$$

In *abz* coordinates, nonlinear polarizations with wave numbers k_{11}, k_{22}, and k_{12} dominate. In particular, near the phase matching condition, the inhomogeneous waves [Eq. (13)] are dominated by k_{12}. In the matrix elements in Eq. (14), the 22 component is normally dominant for relatively small M since q^2/K_0^2 is about L and k_{12} is about $2q$ using the approximation that K_0 is about $q/\sqrt{L}$. In Eq. (14), if only the 22 component is considered,

$$E_{b12}^0 \simeq \frac{-4\pi K_0^4}{(k_{12}-K_1)(k_{12}-K_2)(k_{12}-K_3)(k_{12}-K_4)} \times \left(L - \frac{(k_{12}+q)^2}{K_0^2} \right) P_{b12}^0. \tag{33}$$

The amplitude is infinite under the phase matching condition $k_{12}=K_1$. Using Eqs. (B2)–(B4) and (32),

$$P_{b12}^0 \simeq \left\{ \chi_{bbb} + \chi_{bzz} \left(\frac{\varepsilon_{az}}{\varepsilon_{zz}} \right)^2 \right\} 2a_1 a_2, \tag{34}$$

where χ_{bbb} and χ_{bzz} are given in Appendix B. In *xyz* coordinates, the inhomogeneous wave [Eq. (16)] is expressed as

$$u_p(z) \simeq \frac{1}{\sqrt{2}} \begin{pmatrix} 1 \\ i \\ -i(k_{12}-q)/K_0 \\ (k_{12}-q)/K_0 \end{pmatrix} E_{b12}^0 e^{i(k_{12}-q)z}, \tag{35}$$

which is $(+z,l)$ according to the interpretation of Eq. (25). The boundary condition Eq. (21) determines the homogeneous and emanating SH waves. The right-hand side of Eq. (21) is expressed as

$$-u_p(d) \simeq -u_p(0) e^{i(k_{12}-q)d}, \tag{36}$$

$$-u_p(0) \simeq \frac{1}{\sqrt{2}} \begin{pmatrix} -1 \\ -i \\ i(k_{12}-q)/K_0 \\ -(k_{12}-q)/K_0 \end{pmatrix} E_{b12}^0. \tag{37}$$

The left-hand side of Eq. (21) includes the homogeneous waves. The homogeneous wave with $(+z,l)$ character is mode 1. Under the approximation of $F_1 \simeq 0$, mode 1 is expressed as

$$A_1 \Pi(d)_1 \simeq A_1 \Pi(0)_1 e^{i(K_1-q)d}, \tag{38}$$

$$A_1 \Pi(0)_1 \simeq \frac{1}{\sqrt{2}} \begin{pmatrix} 1 \\ i \\ -i(K_1-q)/K_0 \\ (K_1-q)/K_0 \end{pmatrix} A_1. \tag{39}$$

Near the phase matching condition, we introduce the following simple approximation:

$$\mathbf{A} \simeq \begin{pmatrix} -E_{b12}^0 \\ 0 \\ 0 \\ 0 \end{pmatrix}. \tag{40}$$

Equations (19), (37), (39), and (40) lead to

$$\begin{pmatrix} F_{Lx}^0 \\ F_{Ly}^0 \end{pmatrix} \simeq \begin{pmatrix} 0 \\ 0 \end{pmatrix}, \tag{41}$$

which shows that no SHG comes from the left side. On the other hand, Eqs. (36)–(40) lead to

$$\begin{pmatrix} F_{Rx}^0 \\ F_{Ry}^0 \end{pmatrix} \simeq \sqrt{2} E_{b12}^0 e^{i(k_{12}+K_1-2q)d/2} \sin\frac{(k_{12}-K_1)d}{2} \begin{pmatrix} i \\ -1 \end{pmatrix}, \tag{42}$$

which shows that the SH wave emanating from the right side is of l polarization. The intensity is

$$I = \frac{c\sqrt{\varepsilon_R}}{8\pi} \{ |F_{Rx}^0|^2 + |F_{Ry}^0|^2 \} \simeq \frac{c\sqrt{\varepsilon_R}}{8\pi} \frac{64\pi^2 K_0^8 \{ L - (k_{12}+q)^2/K_0^2 \}^2 \sin^2[(k_{12}-K_1)d/2] |P_{b12}^0|^2}{(k_{12}-K_1)^2(k_{12}-K_2)^2(k_{12}-K_3)^2(k_{12}-K_4)^2} \tag{43}$$

$$= \frac{c\sqrt{\varepsilon_R}}{8\pi} 4 \sin^2\frac{(k_{12}-K_1)d}{2} |E_{b12}^0|^2 \equiv \frac{c\sqrt{\varepsilon_R}}{8\pi} G |E_{b12}^0|^2.$$

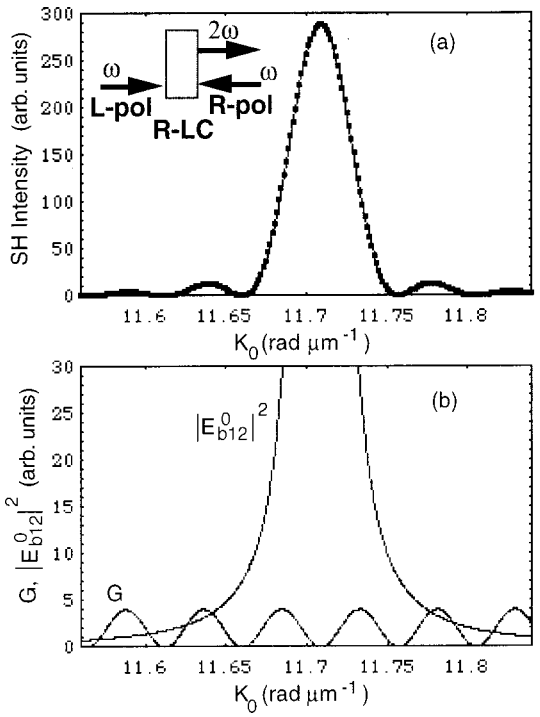

FIG. 4. (a) Phase matching A for $(+z,l;-z,r)$ fundamental waves. Dots, exact theory: curve, Eq. (43) where $|P^0_{b12}|$ is assumed to be constant in this region. (b) $|E^0_{b12}|^2$ and G as functions of K_0.

This is compared with the exact theory [Fig. 4(a)], where the fundamental waves are $(+z,l;-z,r)$, $p=0.358\,761\,84\,\mu$m, $d=87\,\mu$m, and $|P^0_{b12}|$ is assumed to be constant in this region. The approximation is shown to be good. Equation (43) is factored into the form of $G|E^0_{b12}|^2$ and the spectra of G and $|E^0_{b12}|^2$ are shown in Fig. 4(b). G is oscillating. The maximum intensity is approximately obtained under the phase matching condition, where $|E^0_{b12}|^2$ is infinite, while G is zero. In other words, infinite inhomogeneous waves $(+z,l)$ are significantly canceled out by the homogeneous waves $(+z,l)$. The cancellation is complete on the left side. On the right side, $\{\sin^2(k_{12}-K_1)d/2\}/(k_{12}-K_1)^2$ in Eq. (43) varies as $d^2/4$ under the phase matching condition. Thus, phase matching A is conventional in its thickness dependence.

3. Special kind of type-I-like phase matchings B–E

Now let us consider the phase matchings B–E. According to Sec. III B 1, the possible phase matching conditions are $K_0=K_{02}$ or $K_0=K_{013}$. First we concentrate on phase matchings B and D, where the fundamental waves $(+z,r;-z,r)$ are effective. In *abz* coordinates, such fundamental waves are dominated by

$$\begin{pmatrix} E_a \\ E_b \\ E_z \end{pmatrix} \simeq \begin{pmatrix} a_4 f_4 e^{ik_{4^2}z} \\ a_2 e^{ik_{2^2}z} \\ (a_2 e^{ik_{2^2}z} - a_4 f_4 e^{ik_{4^2}z})\varepsilon_{az}/\varepsilon_{zz} \end{pmatrix}. \tag{44}$$

In *abz* coordinates, nonlinear polarizations with wave numbers k_{22}, k_{44}, and $k_{24}=0$ dominate. In particular, near the phase matching conditions, the inhomogeneous waves are expected to be dominated by k_{24} because of the small Δ in Eq. (15). Moreover, E^0_{a24} and E^0_{b24} are dominant because of large 11 (=22) and 12 (=21) components in Eq. (14). In Eq. (14), if only these components are considered,

$$\begin{pmatrix} E^0_{a24} \\ E^0_{b24} \end{pmatrix} \simeq \frac{-4\pi}{\Delta} \begin{pmatrix} L-q^2/K_0^2 & -M \\ -M & L-q^2/K_0^2 \end{pmatrix} \begin{pmatrix} P^0_{a24} \\ P^0_{b24} \end{pmatrix}. \tag{45}$$

Using Eqs. (B2)–(B4) and (44),

$$P^0_{a24} \simeq P^0_{b24} \simeq 2\left\{ \chi_{aaa} - \chi_{abz}\left(\frac{\varepsilon_{az}}{\varepsilon_{zz}}\right) - \chi_{azz}\left(\frac{\varepsilon_{az}}{\varepsilon_{zz}}\right)^2 \right\} a_2 a_4 f_4, \tag{46}$$

and Eq. (45) is reduced to

$$E^0_{a24} \simeq E^0_{b24} \simeq \frac{-4\pi}{\Delta}(L-q^2/K_0^2-M)P^0_{a24} = \frac{4\pi}{q^2/K_0^2-\tilde{\varepsilon}_2} P^0_{a24}. \tag{47}$$

At the λ_2 edge, Eq. (47) is infinite since $q^2/K_{02}^2=\tilde{\varepsilon}_2$, namely, enhanced SHG is expected for the phase matching condition $K_0=K_{02}$. On the other hand, the other condition $K_0=K_{013}$ is not effective since $q^2/K_{013}^2=\tilde{\varepsilon}_e$. Thus, no enhanced SHG is expected near the λ_{13} edge unless the λ_{13} and λ_2 edges are nearly degenerate. According to Eq. (16), E^0_{a24} and E^0_{b24} correspond to $(+z,r)$ and $(-z,r)$, respectively. In *xyz* coordinates, the inhomogeneous wave in Eq. (16) is expressed as

$$u_p(z) \simeq \sqrt{2} \begin{pmatrix} -i\sin qz \\ i\cos qz \\ (q\sin qz)/K_0 \\ -(q\cos qz)/K_0 \end{pmatrix} E^0_{a24}. \tag{48}$$

This wave has the same form as the homogeneous wave at the λ_2 edge [Eq. (29)], namely, it is a standing wave of right-handed helical form whose electric and magnetic fields are always parallel to the C_2 axis. On the other hand, the inhomogeneous wave is orthogonal to the homogeneous wave at the λ_{13} edge [Eq. (30)].

Until now the phase matchings B and D were considered. Now let us consider the phase matchings C and E, where the fundamental waves $(+z,l;-z,l)$ are effective. In *abz* coordinates, such fundamental waves are dominated by

$$\begin{pmatrix} E_a \\ E_b \\ E_z \end{pmatrix} \simeq \begin{pmatrix} a_3 f_3 e^{ik_{3^2}z} \\ a_1 e^{ik_{1^2}z} \\ (a_1 e^{ik_{1^2}z} - a_3 f_3 e^{ik_{3^2}z})\varepsilon_{az}/\varepsilon_{zz} \end{pmatrix}. \tag{49}$$

Following the previous discussion, the inhomogeneous waves are dominated by E^0_{a13} and E^0_{b13} with wave number $k_{13}=0$ and they are expressed as

$$E^0_{a13}\simeq E^0_{b13}\simeq \frac{-4\pi}{\Delta}(L-q^2/K_0^2-M)P^0_{a13}$$

$$=\frac{4\pi}{q^2/K_0^2-\tilde{\varepsilon}_2}P^0_{a13}, \tag{50}$$

where

$$P^0_{a13}\simeq P^0_{b13}\simeq 2\left\{\chi_{aaa}-\chi_{abz}\left(\frac{\varepsilon_{az}}{\varepsilon_{zz}}\right)-\chi_{azz}\left(\frac{\varepsilon_{az}}{\varepsilon_{zz}}\right)^2\right\}a_1a_3f_3. \tag{51}$$

In *xyz* coordinates, the inhomogeneous wave is expressed as

$$u_p(z)\simeq\sqrt{2}\begin{pmatrix} -i\sin qz \\ i\cos qz \\ (q\sin qz)/K_0 \\ -(q\cos qz)/K_0 \end{pmatrix}E^0_{a13}. \tag{52}$$

Since Eqs. (50), (51), and (52) are similar to Eqs. (47), (46), and (48), respectively, phase matchings *C* and *E* occur in similar ways to phase matchings *B* and *D*, respectively. That is, the phase matching is achieved irrespective of the polarization of the fundamental waves, if both are the same (type *I* like) and counterpropagating. The SH wave is enhanced near the λ_2 edge and is *r* polarized. These predictions were actually observed experimentally [15–17], and will be discussed further in the following. To simplify the notations, we proceed with the analysis only for $(+z,r;-z,r)$.

4. Further details of the special phase matching

The homogeneous and emanating SH waves are determined by the boundary conditions. Since the inhomogeneous waves are *r* polarized, the homogeneous waves are assumed to be dominated by *r*-polarized modes 2 and 4. For simplicity, we proceed with the analysis under the following conditions:

$$\varepsilon_R=\varepsilon_L, \tag{53}$$

$$K_0\sqrt{\varepsilon_L}\simeq q, \tag{54}$$

$$K_2\simeq 0. \tag{55}$$

Condition (54) is equivalent to $\sqrt{\varepsilon_L}p\simeq\lambda_0(2\omega)$, namely, ε_L is close to the dielectric constants of LCs. Condition (55) is satisfied when SHG occurs near the edges of the gap. Under these conditions, let us consider a homogeneous wave with the following form as an approximate solution:

$$\mathbf{A}=\begin{pmatrix} 0 \\ A_2 \\ 0 \\ A_2e^{iK_2d}(F_2+1)/(F_4+1) \end{pmatrix}. \tag{56}$$

Here $(F_2+1)/(F_4+1)$ can be transformed to the following relations using Eq. (26):

$$\frac{F_2+1}{F_4+1}=-\frac{-F_2+1}{-F_4+1}=-\frac{F_2(K_2+q)+K_2-q}{F_4(K_4+q)+K_4-q}$$

$$=\frac{-F_2(K_2+q)+K_2-q}{-F_4(K_4+q)+K_4-q}. \tag{57}$$

For Eq. (56), the boundary conditions Eq. (19) are given by

$$\begin{pmatrix} A_2(-F_2+1)(1-e^{iK_2d})/\sqrt{2} \\ A_2i(F_2+1)(1+e^{iK_2d})/\sqrt{2}+\sqrt{2}iE^0_{a24} \\ -A_2i\{F_2(K_2+q)+K_2-q\}(1-e^{iK_2d})/\sqrt{2}K_0 \\ A_2\{-F_2(K_2+q)+K_2-q\}(1+e^{iK_2d})/\sqrt{2}K_0-\sqrt{2}qE^0_{a24}/K_0 \end{pmatrix}=\begin{pmatrix} F^0_{Lx} \\ F^0_{Ly} \\ \sqrt{\varepsilon_L}F^0_{Ly} \\ -\sqrt{\varepsilon_L}F^0_{Lx} \end{pmatrix}, \tag{58}$$

$$\Pi(d)\mathbf{A}+u_p(d)=\begin{pmatrix} -F^0_{Ly} & -F^0_{Lx} \\ -F^0_{Lx} & F^0_{Ly} \\ \sqrt{\varepsilon_L}F^0_{Lx} & -\sqrt{\varepsilon_L}F^0_{Ly} \\ -\sqrt{\varepsilon_L}F^0_{Ly} & -\sqrt{\varepsilon_L}F^0_{Lx} \end{pmatrix}\begin{pmatrix} \sin qd \\ \cos qd \end{pmatrix}=\begin{pmatrix} F^0_{Rx} \\ F^0_{Ry} \\ -\sqrt{\varepsilon_R}F^0_{Ry} \\ \sqrt{\varepsilon_R}F^0_{Rx} \end{pmatrix} \tag{59}$$

(see Appendix C). Using Eq. (53), Eq. (59) is simplified to

$$F^0_{Rx}=-\cos qdF^0_{Lx}-\sin qdF^0_{Ly},$$

$$F^0_{Ry}=-\sin qdF^0_{Lx}+\cos qdF^0_{Ly}. \tag{60}$$

The boundary conditions are now reduced to Eqs. (58) and (60). If we eliminate F^0_{Lx} and F^0_{Ly} in Eq. (58), we obtain the relations.

$$A_2=\frac{-2qE^0_{a24}}{-K_0\sqrt{\varepsilon_L}(-F_2+1)+q(F_2+1)+K_2(F_2-1)+e^{iK_2d}\{K_0\sqrt{\varepsilon_L}(-F_2+1)+q(F_2+1)+K_2(F_2-1)\}}, \tag{61}$$

$$A_2=\frac{-2K_0\sqrt{\varepsilon_L}E^0_{a24}}{K_0\sqrt{\varepsilon_L}(F_2+1)-q(-F_2+1)+K_2(F_2+1)+e^{iK_2d}\{K_0\sqrt{\varepsilon_L}(F_2+1)+q(-F_2+1)-K_2(F_2+1)\}}, \tag{62}$$

respectively. Since the assumed relation, Eq. (56), is not exact, the slightly different expressions, Eqs. (61) and (62), are obtained. However, under the conditions of Eqs. (54) and (55), Eqs. (61) and (62) are approximately the same, namely, an approximate solution is obtained. Using Eq. (58), F^0_{Lx} and F^0_{Ly} are expressed as

$$\begin{aligned} F^0_{Lx}&\simeq\frac{A_2(-F_2+1)}{\sqrt{2}}(1-e^{iK_2d}),\\ F^0_{Ly}&\simeq-\frac{A_2i\{F_2(K_2+q)+K_2-q\}}{\sqrt{2}K_0\sqrt{\varepsilon_L}}(1-e^{iK_2d}). \end{aligned} \tag{63}$$

A polarization experiment for ROLIC6304 showed that the SH waves generated by $(+z,r;-z,r)$ and $(+z,l;-z,l)$ are dominated by r polarization [17]. r and l components for the SH waves emanating from the right side are given by

$$\begin{aligned} \begin{pmatrix} F^0_{Rr\,\mathrm{pol}}\\ F^0_{Rl\,\mathrm{pol}}\end{pmatrix}&=\frac{1}{2}\begin{pmatrix}1 & i\\ 1 & -i\end{pmatrix}\begin{pmatrix}F^0_{Rx}\\ F^0_{Ry}\end{pmatrix}\\ &=\frac{A_2(1-e^{iK_2d})}{2\sqrt{2}K_0\sqrt{\varepsilon_L}}\begin{pmatrix}\{(K_0\sqrt{\varepsilon_L}+q)(F_2-1)+K_2(F_2+1)\}e^{iqd}\\ \{(K_0\sqrt{\varepsilon_L}-q)(F_2-1)-K_2(F_2+1)\}e^{-iqd}\end{pmatrix}, \end{aligned} \tag{64}$$

using Eqs. (60) and (63). Under the conditions of Eqs. (54) and (55), the SH wave is dominated by r polarization, which agrees with the experiment.

The SH intensities (I) emanating from l and r sides are

$$I\equiv\frac{c\sqrt{\varepsilon_L}}{8\pi}(|F^0_{Lx}|^2+|F^0_{Ly}|^2)=\frac{c\sqrt{\varepsilon_R}}{8\pi}(|F^0_{Rx}|^2+|F^0_{Ry}|^2), \tag{65}$$

where Eqs. (53) and (60) were used to lead to the second equality. If A_2 is evaluated by Eq. (61) and Eq. (63) is used, in region III, where SHG is outside the gap,

$$I=\frac{c\sqrt{\varepsilon_L}}{8\pi}\frac{(2q^2/K_0^2\varepsilon_L)\{(1/K_0^2\varepsilon_L)[q+K_2(F_2+1)/(F_2-1)]^2+1\}}{[(\cot^2K_2d/2)/K_0^2\varepsilon_L][q(F_2+1)/(F_2-1)+K_2]^2+1}|E^0_{a24}|^2\equiv\frac{c\sqrt{\varepsilon_L}}{8\pi}G|E^0_{a24}|^2, \tag{66}$$

where we used the fact that K_2 and F_2 are real. On the other hand, in region I where SHG is inside the gap.

$$I=\frac{c\sqrt{\varepsilon_L}}{8\pi}\frac{(2q^2/K_0^2\varepsilon_L)\{(1/K_0^2\varepsilon_L)[q+s\cot(\phi/2)]^2+1\}}{[(\coth^2sd/2)/K_0^2\varepsilon_L][q\cot(\phi/2)-s]^2+1}|E^0_{a24}|^2\equiv\frac{c\sqrt{\varepsilon_L}}{8\pi}G|E^0_{a24}|^2, \tag{67}$$

where we used Eqs. (27) and (28) and $\cot(\phi/2)$ is expressed as

$$\cot\frac{\phi}{2}=\frac{-2sq}{(M+L)K_0^2-q^2+s^2}. \tag{68}$$

In Eqs. (66) and (67), $|E^0_{a24}|^2$ is given by

$$|E^0_{a24}|^2=\frac{16\pi^2|P^0_{a24}|^2}{(q^2/K_0^2-\tilde{\varepsilon}_2)^2}. \tag{69}$$

By substituting K_2 [Eq. (27)] and F_2 [Eq. (28)] in Eq. (66), Eq. (67) is reproduced. So Eq. (67) is considered as a special form of Eq. (66). Conversely, by substituting s [Eq. (27)] in Eqs. (67) and (68), Eq. (66) is reproduced, where the relation

$$\frac{F_2+1}{F_2-1}=\frac{2K_2q}{(M+L)K_0^2-q^2-K_2^2}, \tag{70}$$

exists using Eqs. (A7) and (5). Although Eqs. (66) and (67) can be unified, the present forms are simple since only real variables are used. It is noted that these equations for I differ from the conventional case, Eq. (43).

The linear reflectance and SH spectra were calculated near the photonic band gap (Fig. 5). In the linear spectrum, the selective reflection band appears between the λ_{13} and λ_2 edges when a r-polarized wave is incident [19,20]. Multiple reflections of modes 2 and 4 result in subsidiary oscillations near the edges. Such oscillations have actually been observed in some carefully prepared cholesteric cells [24,25]. On the

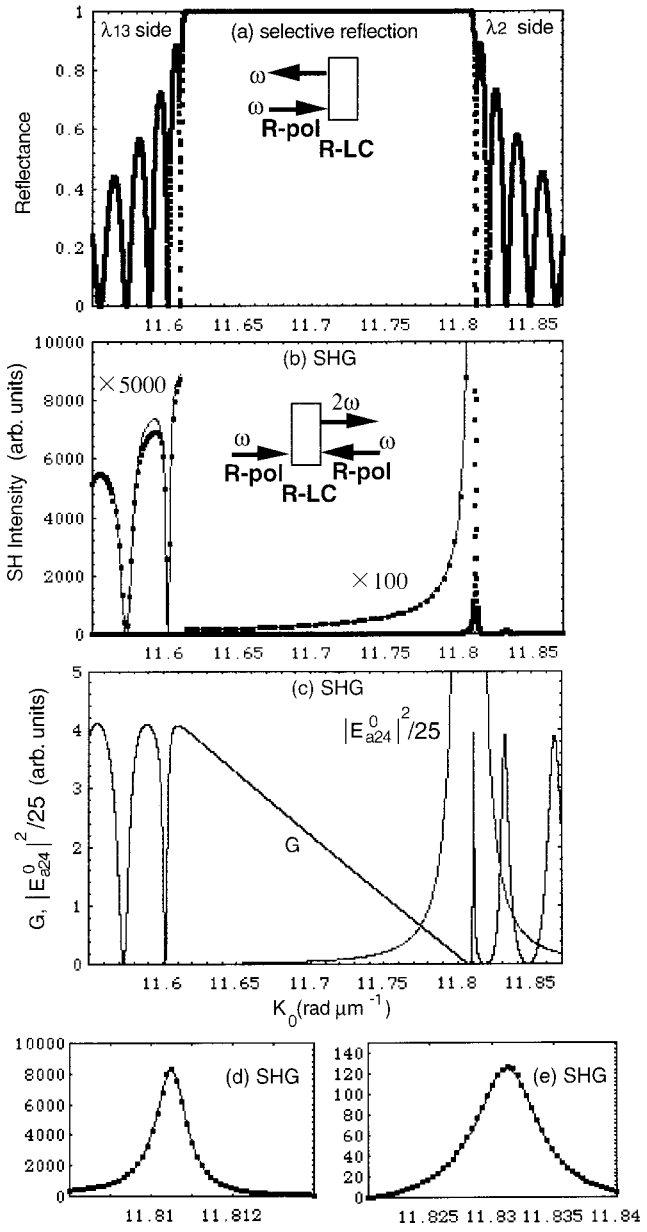

FIG. 5. (a) Linear reflection spectrum by the exact theory for *r*-polarized incident wave. (b) SH spectrum for $(+z,r;-z,r)$ fundamental waves. Except for the polarizations of the fundamental waves, the parameters are identical with those in Fig. 4. Dots, exact theory: curves, Eqs. (66) and (67) under the approximation that $|P^0_{a24}|$ is constant in this region, taken at $K_0 = 11.810\,499$ rad μm^{-1} as a typical value. Regions near the λ_2 edge are enlarged in (d) and (e). (c) $|E^0_{a24}|^2$ and G versus K_0 using Eqs. (66), (67), and (69).

other hand, the SH spectra in Figs. 5(b), 5(d), and 5(e) show that (1) SHG is significantly enhanced only near the λ_2 edge, (2) Eqs. (66) and (67) are good approximations, and (3) the peaks and dips in the SH spectra are located at the dips in the subsidiary oscillations in the selective reflection spectrum.

Equations (66) and (67) were factored into the form of $G|E^0_{a24}|^2$ and their spectra are shown in Fig. 5(c). As noted before, $|E^0_{a24}|^2$ is infinite at the λ_2 edge, but not at the λ_{13}

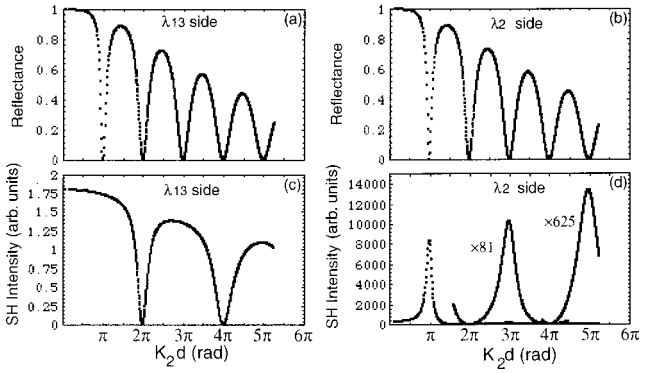

FIG. 6. (a), (b) Linear reflection spectrum in Fig. 5(a), and (c),(d) SH spectrum in Fig. 5(b) are shown as functions of K_2d.

edge. Thus, SHG is enhanced only near the λ_2 edge unless λ_{13} and λ_2 are nearly degenerate. In Fig. 5(c), G is a monotonic function in region *I* and oscillating in region III, which differs from G for phase matching *A*. For phase matching *A*, the maximum intensity is realized under the condition that $|E^0_{b12}|^2$ is infinite, although G is zero. For the present case, a similar situation occurs under the phase matching condition $K_0 = K_{02}$, namely, at the λ_2 edge, where $|E^0_{a24}|^2$ is infinite and G is zero since $K_0 = K_{02} = q/\sqrt{L+M}$, $K_2(F_2+1)/(F_2-1) \rightarrow -qM/(L+M)$, $q(F_2+1)/(F_2-1) \rightarrow \infty$, and $\cot^2 K_2 d/2 \rightarrow \infty$. At the λ_2 edge, the infinite amplitude of the inhomogeneous wave Eq. (48) is canceled by the infinite homogeneous wave Eq. (29), and the emanating SHG is comparable to that for phase matching *A* [see Figs. 4(a) and 5(b)].

As noted above, the peaks and dips in the SH spectra are located at the dips in the selective reflection band. This relation is clear in Fig. 6, where the selective reflection and SH spectra are shown as a function of K_2d. In the linear spectra, the dips are located at

$$K_2 d = n\pi, \tag{71}$$

where n are positive integers. On the other hand, in the SH spectra, the peaks are located at

$$K_2 d = N\pi, \tag{72}$$

where N are odd integers, while the dips are located at

$$K_2 d = N'\pi, \tag{73}$$

where N' are even integers, which shows that the locations of the peaks and dips are determined by G. According to a previous paper, n (N,N') corresponds to the number of wave packets for the homogeneous waves in the cell [18]. When an even number of wave packets are produced, the inhomogeneous wave is canceled by the homogeneous waves at the boundary. According to Eq. (63), the cancellation is perfect for the condition $K_2 d = N'\pi$. On the other hand, when an odd number of wave packets are produced, the cancellation at the boundary is decreased and significant SHG emanates from the cell. These relations are shown graphically in Figs. 5 and 6 in Ref. [18]. Experimentally, at present, the difficulty

in preparing high quality cells prevents the observation of the dips in ROLIC6304 and such relations between SHG and selective reflections have not been confirmed yet.

5. Cell thickness dependence of SH intensity and width

To estimate the maximum I near the λ_2 edge using Eq. (66), we assume that $K_2(F_2+1)/(F_2-1)$ in the numerator and K_2 in $q(F_2+1)/(F_2-1)+K_2$ in the denominator are negligible,

$$I \simeq \frac{c\sqrt{\varepsilon_L}}{8\pi} \times \frac{(2q^2/K_0^2\varepsilon_L)[(q^2/K_0^2\varepsilon_L)+1]}{[(\cot^2 K_2 d/2)/K_0^2\varepsilon_L][q(F_2+1)/(F_2-1)]^2+1} \times |E_{a24}^0|^2. \tag{74}$$

Moreover, we assume that I has its maximum value $I_{\max}$ under the condition $K_2 d = N\pi$, namely, $\cot^2 K_2 d/2 = 0$. Now we consider Eq. (74) as a function of q and d since previous experiments were carried out under the condition that K_0 was fixed and the pitch and thickness were varied. To express the condition showing the maximum I in an approximate form, it is convenient to introduce δ. As noted previously, M for ROLIC6304 is negative and K_{02} is larger than K_{013}. To express region III near the K_{02} edge for negative M, δ (>0) is defined as

$$q \equiv K_0\sqrt{L+M} - \delta. \tag{75}$$

For small δ, K_2 can be expressed in the following series:

$$K_2 = \Big[K_0^2(2L+M) - 2K_0\sqrt{L+M}\,\delta + \delta^2 - \sqrt{K_0^4(2L+M)^2 - 8K_0^3 L\sqrt{L+M}\,\delta + 4K_0^2 L\delta^2}\Big]^{1/2} \simeq \sqrt{\delta}(C_0 + C_1\delta + \cdots), \tag{76}$$

where

$$C_0 = \sqrt[4]{L+M}\sqrt{-2K_0 M/(2L+M)}, \qquad C_1 = \frac{1}{2C_0}\left\{1 - \frac{2LM^2}{(2L+M)^3}\right\}. \tag{77}$$

C_0 is about 0.5 in our case. If only the first term is considered, $K_2 d = N\pi$ is expressed as

$$q_{\max} = K_0\sqrt{L+M} - \frac{N^2\pi^2}{C_0^2 d^2}, \tag{78}$$

where $q_{\max}$ is the q value that corresponds to the maximum I. As shown in this equation, $q_{\max}$ converges to $K_0\sqrt{L+M}$ at infinite d. Figure 7(a) confirms these expectations, where $q_{\max}$ is numerically obtained from the peak of I versus q using the exact theory and shown as a function of thickness. The denominator of Eq. (69) for $q_{\max}$ is

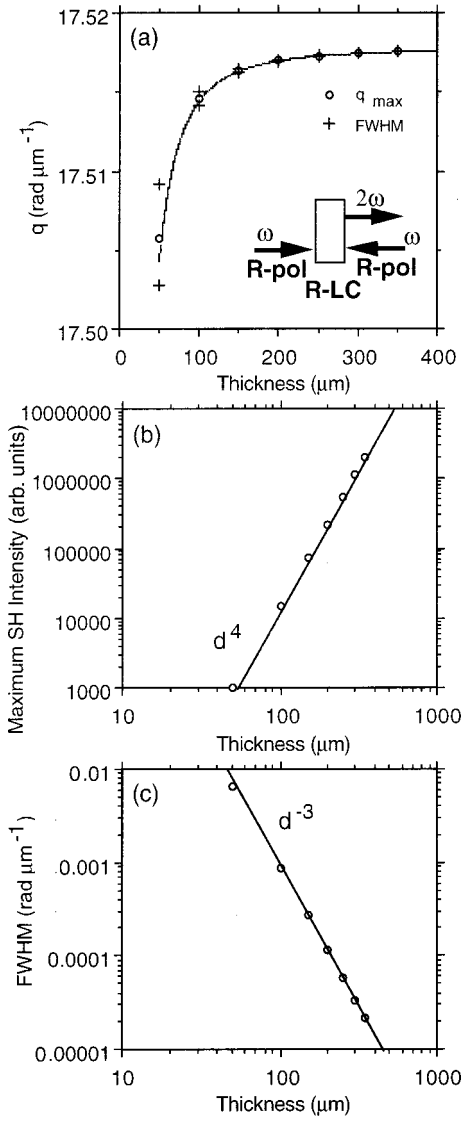

FIG. 7. (a) Thickness dependence of the peak position and width for the SHG peaks ($N=1$). $q_{\max}$ ($\bigcirc$) is the location of the SHG peak and FWHM ($+$) is the location of q that corresponds to the FWHM for the SHG peak. They are numerically calculated by the exact theory using identical parameters to those in Fig. 5(b) except $\lambda_0(\omega) = 1.064\,\mu$m. The curve is drawn based on approximate Eq. (78). (b) Thickness dependence of the maximum SHG intensity ($N=1$) calculated by the exact theory. The results are well fitted to the d^4 dependence (straight line). The locations of q are shown in (a). (c) Thickness dependence of FWHM ($N=1$) calculated by the exact theory. FWHM is obtained from (a). The results are well fitted to the d^{-3} dependence (straight line). The locations of the FWHM are shown in (a).

$$\left(\frac{q_{\max}^2}{K_0^2} - \tilde{\varepsilon}_2\right)^2 = \left(-\frac{2\sqrt{L+M}N^2\pi^2}{K_0 C_0^2 d^2} + \frac{N^4\pi^4}{K_0^2 C_0^4 d^4}\right)^2 \simeq \frac{4(L+M)N^4\pi^4}{K_0^2 C_0^4 d^4}, \tag{79}$$

where we assume that d is relatively large. Moreover, for

such d values, $q^2/(K_0^2\varepsilon_L)$ terms are evaluated approximately by using

$$q_{\max}^2 \simeq K_0^2(L+M). \tag{80}$$

Under these approximations, $I_{\max}$ is expressed as

$$I_{\max} \simeq \frac{c\sqrt{\varepsilon_L}}{8\pi}\frac{2\tilde{\varepsilon}_2}{\varepsilon_L}\left(\frac{\tilde{\varepsilon}_2}{\varepsilon_L}+1\right)\frac{4K_0^2C_0^4d^4}{\tilde{\varepsilon}_2\pi^2N^4}|P_{a24}^0|^2. \tag{81}$$

Thus, $I_{\max}$ is d^4 and N^{-4} dependent. The N^{-4} dependence is roughly shown in Fig. 6(d). The thickness dependence of $I_{\max}$ is shown in Fig. 7(b), which verifies the d^4 dependence. This d^4 dependence is the advantageous point of the special phase matching [7,10]. In a previous paper [10], Yoo *et al.* carried out a simulation using the analytical theory by Copic and Drevensek-Olenik [9] and showed that $I_{\max}$ is d^4 dependent. In the present paper, this characteristic is shown analytically based on the exact theory.

For the SHG peaks as a function of q, the full width at half maximum (FWHM) is also thickness dependent. In Eq. (74), half values of $I_{\max}$ are obtained when

$$\frac{\cot^2(K_2d/2)}{K_0^2\varepsilon_L}\left(q\frac{F_2+1}{F_2-1}\right)^2 \simeq 1. \tag{82}$$

Moreover, when $K_2d/2$ is close to $N\pi/2$,

$$\cot^2\frac{K_2d}{2} \simeq \left(\frac{K_2d}{2}-\frac{N\pi}{2}\right)^2 \simeq \left(\frac{C_0\sqrt{\delta}d}{2}-\frac{N\pi}{2}\right)^2. \tag{83}$$

Furthermore, for small δ,

$$\begin{aligned}\left(q\frac{F_2+1}{F_2-1}\right)^2 &= \frac{4K_2^2q^4}{\{(M+L)K_0^2-q^2-K_2^2\}^2} \\ &\simeq \frac{-8K_0^5M(L+M)^{5/2}\delta/(2L+M)+\cdots}{16K_0^2(L+M)^3\delta^2/(2L+M)^2+\cdots} \\ &\simeq \frac{K_0^4M^2}{C_0^2\delta}.\end{aligned} \tag{84}$$

Using Eqs. (83) and (84), two approximate solutions for δ, δ_1 and δ_2, for Eq. (82) satisfy

$$\delta_1-\delta_2 = \frac{8C_0^2\sqrt{\varepsilon_L}\pi^2N^2d}{-K_0M(C_0^2d^2-4C_0^2\varepsilon_L/K_0^2M^2)^2}. \tag{85}$$

In the denominator of Eq. (85), the first term is dominant if d is relatively large. Thus, the FWHM is d^{-3} and N^2 dependent in a thick cell,

$$\delta_1-\delta_2 \simeq \frac{4\sqrt{\varepsilon_L}(2L+M)\pi^2N^2}{K_0^2M^2\sqrt{L+M}d^3}. \tag{86}$$

Such a d^{-3} dependence was also noted by Belyakov and Shipov [7]. The thickness dependence of the FWHM is shown in Fig. 7(b), which verifies the d^{-3} dependence. The FWHM for the special phase matching is much narrower than that for the conventional one [Figs. 4(a) and 5(b)]. For a 100 μm thick ROLIC6304 cell, the FWHM is $\Delta q = 8.82 \times 10^{-4}$ rad μm^{-1}. This corresponds to $\Delta p = 0.018$ nm when p is varied instead of q. For applications, the requirement of such high stability is the problematic point of special phase matching.

In summary, two types of phase matching condition have been described. Both are due to SHG using counterpropagating fundamental waves. The first type is for the incidence of r- and l-polarized waves. It was found that phase matched SHG occurs along the direction where the r-polarized wave is incident. That is, the propagation direction of the phase matched SH wave is the same as the propagation direction of the fundamental l-polarized wave. It was also found that the phase matched SH wave is l polarized and the process is described by Fig. 3 type *A*, including an umklapp process. In the present analysis, the SH intensity in this process is described by an expression [Eq. (43)] similar to that for the usual phase matched SH intensity, and depends on the square of the sample thickness, d^2.

The second type of phase matching condition is for the incidence of light of the same polarization. The phase matched SHG is very characteristic in many ways.

(1) The phase matching occurs near one of the edges (λ_2 edge) of a photonic gap (selective reflection band). In the present case (negative M), it is near the higher energy edge. This situation is clear in Eqs. (47) and (50).

(2) The exact position showing the maximum SH intensity corresponds to the first dip position of the subsidiary oscillation in the higher energy region of the selective reflection, so that the peak position shifts toward the λ_2 edge with increasing cell thickness.

(3) Because of the shift, the dependence of the SH intensity on the cell thickness is quite special, i.e., d^4. This is explained as follows. The inhomogeneous wave E_{a24}^0 is expressed by Eq. (47). If we define ΔK_0 as K_0 measured from the edge K_{02}, it is readily found that E_{a24}^0 is proportional to ΔK_0. On the other hand, ΔK_0 is proportional to K_2^2, since the dispersion curve near zero K_2 is approximated by a parabolic function. Using $K_2d = N\pi$, ΔK_0 is proportional to d^2. Then finally we reach the conclusion that the maximum SH intensity [proportional to $(E_{a24}^0)^2$] occurs at the first dip of the subsidiary oscillation in the selective reflection and depends on d^4. A physically intuitive interpretation concerns the dispersion relation, since the group velocity of the SH wave becomes slow near the edge, indicating stronger nonlinear interaction.

IV. CONCLUSION

The special phase matching process was analyzed. The numerical results obtained from the exact theory were expressed in simple analytical forms. It was shown that two counterpropagating waves in $(+z,r;-z,r)$ and $(+z,l;-z,l)$ polarizations lead to special phase matching. The relation between the selective reflection and SHG spectra was also pointed out. The maximum SH intensity occurs at the first dip on the λ_2 side of the selective reflection spectrum. In thick cells, the maximum SH intensity is d^4 dependent, while

the conventional phase matching is d^2 dependent. However, since the FWHM is d^{-3} dependent, extremely stable LC cells are required to realize the d^4 dependence of the SH intensity.

ACKNOWLEDGMENT

We acknowledge fruitful discussions with Professor V. A. Belyakov, L. D. Landau Institute of Theoretical Physics, Moscow, Russia.

APPENDIX A

Equations (3)–(6) are derived. In *abz* coordinates, Eq. (1) is transformed to

$$W_{\alpha i}(-\partial_z^2 I_{ij}^0 - k_0^2 \varepsilon'_{ij})(W^{-1})_{j\beta} E_\beta = 0. \tag{A1}$$

We define $\varepsilon_{\alpha\beta}$ as

$$\varepsilon_{\alpha\beta} \equiv W_{\alpha i}(W^{-1})_{j\beta}\varepsilon'_{ij} = W_{\alpha i}(W^{-1})_{j\beta} R_{ip} R_{jq} \varepsilon_{pq}, \tag{A2}$$

given by

$$\begin{aligned}
\varepsilon_{aa} &= \varepsilon_{bb} = \{\varepsilon_1 + 2\varepsilon_2 + \varepsilon_3 + (\varepsilon_1 - \varepsilon_3)\cos 2\theta\}/4, \\
\varepsilon_{ab} &= \varepsilon_{ba} = \{-\varepsilon_1 + 2\varepsilon_2 - \varepsilon_3 + (\varepsilon_3 - \varepsilon_1)\cos 2\theta\}/4, \\
\varepsilon_{az} &= \varepsilon_{za} = -\varepsilon_{bz} = -\varepsilon_{zb} = (\varepsilon_1 - \varepsilon_3)\sin 2\theta/2\sqrt{2}, \\
\varepsilon_{zz} &= \varepsilon_1 \sin^2\theta + \varepsilon_3 \cos^2\theta.
\end{aligned} \tag{A3}$$

Using the relation

$$-W_{\alpha i}\partial_z^2 I_{ij}^0 (W^{-1})_{j\beta} = \begin{pmatrix} (q - i\partial_z)^2 & 0 & 0 \\ 0 & (q + i\partial_z)^2 & 0 \\ 0 & 0 & 0 \end{pmatrix},$$

Eq. (A1) is expressed as

$$\begin{pmatrix} (q - i\partial_z)^2 - k_0^2\varepsilon_{aa} & -k_0^2\varepsilon_{ab} & -k_0^2\varepsilon_{az} \\ -k_0^2\varepsilon_{ba} & (q + i\partial_z)^2 - k_0^2\varepsilon_{bb} & -k_0^2\varepsilon_{bz} \\ -k_0^2\varepsilon_{za} & -k_0^2\varepsilon_{zb} & -k_0^2\varepsilon_{zz} \end{pmatrix} \begin{pmatrix} E_a \\ E_b \\ E_z \end{pmatrix} = 0, \tag{A4}$$

which is reduced to

$$\begin{aligned}
E_z &= -\frac{1}{\varepsilon_{zz}}(\varepsilon_{za} \;\; \varepsilon_{zb}) \begin{pmatrix} E_a \\ E_b \end{pmatrix}, \\
&\begin{pmatrix} (q - i\partial_z)^2 - k_0^2 l & -k_0^2 m \\ -k_0^2 m & (q + i\partial_z)^2 - k_0^2 l \end{pmatrix} \begin{pmatrix} E_a \\ E_b \end{pmatrix} = 0,
\end{aligned} \tag{A5}$$

where l and m are given by Eq. (6). The solutions for Eq. (A5) are given by

$$\begin{pmatrix} E_a \\ E_b \end{pmatrix} = \begin{pmatrix} E_a^0 \\ E_b^0 \end{pmatrix} e^{ikz}, \tag{A6}$$

which leads to

$$\begin{pmatrix} (k+q)^2 - k_0^2 l & -k_0^2 m \\ -k_0^2 m & (k-q)^2 - k_0^2 l \end{pmatrix} \begin{pmatrix} E_a \\ E_b \end{pmatrix} = 0. \tag{A7}$$

Thus, $k, E_a/E_b$, and the general solutions are given by Eqs. (4), (5), and (3), respectively.

APPENDIX B

Equations (12)–(16) are derived. In *xyz* coordinates, Eq. (11) is expressed in the same way as Eq. (1),

$$(-\partial_z^2 I_{ij}^0 - K_0^2 \tilde{\varepsilon}'_{ij}) E'_j = 4\pi K_0^2 P'_i, \tag{B1}$$

where the time factor $e^{-i2\omega t}$ is eliminated. $\tilde{\varepsilon}'_{ij}$, E'_j, and P'_i are the components in *xyz* coordinates. To express it in *abz* coordinates, we define P_α and $\chi_{\alpha\beta\gamma}$ as

$$\begin{aligned}
P_\alpha &= W_{\alpha i} P'_i = W_{\alpha i}\chi'_{ijk} E'_j E'_k \\
&= W_{\alpha i}(W^{-1})_{j\beta}(W^{-1})_{k\gamma}\chi'_{ijk} E_\beta E_\gamma = \chi_{\alpha\beta\gamma} E_\beta E_\gamma,
\end{aligned} \tag{B2}$$

$$\begin{aligned}
\chi_{\alpha\beta\gamma} &= W_{\alpha i}(W^{-1})_{j\beta}(W^{-1})_{k\gamma}\chi'_{ijk} \\
&= W_{\alpha i}(W^{-1})_{j\beta}(W^{-1})_{k\gamma} R_{ip} R_{jq} R_{kr} \chi_{pqr},
\end{aligned} \tag{B3}$$

where χ'_{ijk} are the components in *xyz* coordinates. $\chi_{\alpha\beta\gamma}$ are expressed as

$$\begin{aligned}
\chi_{aaa} &= \chi_{aab} = \chi_{aba} = \chi_{bab} = \chi_{bba} = \chi_{bbb} \\
&= i\{\chi_{112} + 2\chi_{222} + \chi_{332} + (\chi_{112} - \chi_{332})\cos 2\theta \\
&\quad + 2\chi_{132}\sin 2\theta\}/4\sqrt{2}, \\
\chi_{azz} &= \chi_{bzz} = -\chi_{zaz} = -\chi_{zbz} = -\chi_{zza} = -\chi_{zzb} \\
&= i\{-\chi_{112} - \chi_{332} + (\chi_{112} - \chi_{332})\cos 2\theta \\
&\quad + 2\chi_{132}\sin 2\theta\}/2\sqrt{2}, \\
\chi_{abb} &= \chi_{baa} = i\{-3\chi_{112} + 2\chi_{222} - 3\chi_{332} + (3\chi_{332} \\
&\quad - 3\chi_{112})\cos 2\theta - 6\chi_{132}\sin 2\theta\}/4\sqrt{2}, \\
\chi_{abz} &= \chi_{azb} = \chi_{zaa} = -\chi_{baz} = -\chi_{bza} = -\chi_{zbb} \\
&= i\{-2\chi_{132}\cos 2\theta + (\chi_{112} - \chi_{332})\sin 2\theta\}/2, \\
\chi_{aaz} &= \chi_{aza} = \chi_{bbz} = \chi_{bzb} = \chi_{zab} = \chi_{zba} = \chi_{zzz} = 0.
\end{aligned} \tag{B4}$$

In *abz* coordinates, Eq. (B1) is transformed in the same way as Eq. (A4).

$$\begin{pmatrix} (q-i\partial_z)^2-K_0^2\tilde{\varepsilon}_{aa} & -K_0^2\tilde{\varepsilon}_{ab} & -K_0^2\tilde{\varepsilon}_{az} \\ -K_0^2\tilde{\varepsilon}_{ba} & (q+i\partial_z)^2-K_0^2\tilde{\varepsilon}_{bb} & -K_0^2\tilde{\varepsilon}_{bz} \\ -K_0^2\tilde{\varepsilon}_{za} & -K_0^2\tilde{\varepsilon}_{zb} & -K_0^2\tilde{\varepsilon}_{zz} \end{pmatrix} \times \begin{pmatrix} E_a \\ E_b \\ E_z \end{pmatrix} = 4\pi K_0^2 \begin{pmatrix} P_a \\ P_b \\ P_z \end{pmatrix}, \tag{B5}$$

where $\tilde{\varepsilon}_{\alpha\beta}$ are defined as in Eq. (A3) using the dielectric constants at 2ω. Thus, the inhomogeneous wave is given by Eqs. (13)–(15).

APPENDIX C

Equations (58) and (59) are derived. For Eq. (56), the homogeneous wave Eq. (17) is expressed as

$$\Pi(0)\mathbf{A}=\frac{A_2}{\sqrt{2}}\begin{pmatrix} (-F_2+1)(1-e^{iK_2d}) \\ i(F_2+1)(1+e^{iK_2d}) \\ -i\{F_2(K_2+q)+K_2-q\}(1-e^{iK_2d})/K_0 \\ \{-F_2(K_2+q)+K_2-q\}(1+e^{iK_2d})/K_0 \end{pmatrix} \tag{C1}$$

at $z=0$. Thus, Eq. (58) is obtained. Also, using the relations

$$A_2\Pi(d)_2=\frac{A_2e^{iK_2d}}{\sqrt{2}}\begin{pmatrix} -i(F_2+1) & -F_2+1 \\ -F_2+1 & i(F_2+1) \\ -\{-F_2(K_2+q)+K_2-q\}/K_0 & -i\{F_2(K_2+q)+K_2-q\}/K_0 \\ -i\{F_2(K_2+q)+K_2-q\}/K_0 & \{-F_2(K_2+q)+K_2-q\}/K_0 \end{pmatrix}\begin{pmatrix} \sin qd \\ \cos qd \end{pmatrix}, \tag{C2}$$

$$A_4\Pi(d)_4=\frac{A_4e^{iK_4d}}{\sqrt{2}}\begin{pmatrix} -i(F_4+1) & -F_4+1 \\ -F_4+1 & i(F_4+1) \\ -\{-F_4(K_4+q)+K_4-q\}/K_0 & -i\{F_4(K_4+q)+K_4-q\}/K_0 \\ -i\{F_4(K_4+q)+K_4-q\}/K_0 & \{-F_4(K_4+q)+K_4-q\}/K_0 \end{pmatrix}\begin{pmatrix} \sin qd \\ \cos qd \end{pmatrix},$$

$$=\frac{A_2}{\sqrt{2}}\begin{pmatrix} -i(F_2+1) & -(-F_2+1) \\ -(-F_2+1) & i(F_2+1) \\ -\{-F_2(K_2+q)+K_2-q\}/K_0 & i\{F_2(K_2+q)+K_2-q\}/K_0 \\ i\{F_2(K_2+q)+K_2-q\}/K_0 & \{-F_2(K_2+q)+K_2-q\}/K_0 \end{pmatrix}\begin{pmatrix} \sin qd \\ \cos qd \end{pmatrix}, \tag{C3}$$

$$\Pi(d)\mathbf{A}=\frac{A_2}{\sqrt{2}}\begin{pmatrix} -i(F_2+1)(1+e^{iK_2d}) & -(-F_2+1)(1-e^{iK_2d}) \\ -(-F_2+1)(1-e^{iK_2d}) & i(F_2+1)(1+e^{iK_2d}) \\ -\{-F_2(K_2+q)+K_2-q\}(1+e^{iK_2d})/K_0 & i\{F_2(K_2+q)+K_2-q\}(1-e^{iK_2d})/K_0 \\ i\{F_2(K_2+q)+K_2-q\}(1-e^{iK_2d})/K_0 & \{-F_2(K_2+q)+K_2-q\}(1+e^{iK_2d})/K_0 \end{pmatrix}\begin{pmatrix} \sin qd \\ \cos qd \end{pmatrix}, \tag{C4}$$

$$u_p(d)\simeq\sqrt{2}E^0_{a24}\begin{pmatrix} -i & 0 \\ 0 & i \\ q/K_0 & 0 \\ 0 & -q/K_0 \end{pmatrix}\begin{pmatrix} \sin qd \\ \cos qd \end{pmatrix}, \tag{C5}$$

and Eq. (58), Eq. (59) is obtained.

[1] E. Yablonovitch and T. J. Gmitter, Phys. Rev. Lett. **63**, 1950 (1989).
[2] M. Scalora, M. J. Bloemer, A. S. Manka, J. P. Dowling, C. M. Bowden, R. Viswanathan, and J. W. Haus, Phys. Rev. A **56**, 3166 (1997).
[3] J. W. Haus, R. Viswanathan, M. Scalora, A. G. Kalocsai, J. D. Cole, and J. Theimer, Phys. Rev. A **57**, 2120 (1998).
[4] J. W. Shelton and Y. R. Shen, Phys. Rev. Lett. **25**, 23 (1970).
[5] J. W. Shelton and Y. R. Shen, Phys. Rev. Lett. **26**, 538 (1971).
[6] J. W. Shelton and Y. R. Shen, Phys. Rev. A **5**, 1867 (1972).
[7] V. A. Belyakov and N. V. Shipov, Phys. Lett. **86A**, 94 (1981).
[8] V. A. Belyakov and N. V. Shipov, Zh. Eksp. Teor. Fiz. [Sov. Phys. JETP **55**, 674 (1982)].
[9] M. Copic and I. Drevensek-Olenik, Liq. Cryst. **21**, 233 (1996).
[10] J.-G. Yoo, S.-W. Choi, H. Hoshi, K. Ishikawa, H. Takezoe, and M. Schadt, Jpn. J. Appl. Phys., Part 2 **36**, L1168 (1997).
[11] V. A. Belyakov, Pis'ma Zh. Eksp. Teor. Fiz. [JETP Lett. **70**, 811 (1999)].

[12] K. Kajikawa, T. Isozaki, H. Takezoe, and A. Fukuda, Jpn. J. Appl. Phys., Part 2 **31**, L679 (1992).
[13] T. Furukawa, T. Yamada, K. Ishikawa, H. Takezoe, and A. Fukuda, Appl. Phys. B: Lasers Opt. **60**, 485 (1995).
[14] I. Drevensek-Olenik and M. Copic, Phys. Rev. E **56**, 581 (1997).
[15] H. Hoshi, D.-H. Chung, K. Ishikawa, and H. Takezoe, Nonlinear Opt. **22**, 95 (1999).
[16] H. Hoshi, D.-H. Chung, K. Ishikawa, and H. Takezoe, Bull. Mater. Sci. **22**, 439 (1999).
[17] D.-H. Chung, H. Hoshi, K. Ishikawa, H. Takezoe, and M. Schadt, Mol. Cryst. Liq. Cryst. Sci. Technol., Sect. A **328**, 283 (1999).
[18] H. Hoshi, D.-H. Chung, K. Ishikawa, and H. Takezoe, Proc. SPIE **3955**, 58 (2000).
[19] V. A. Belyakov and V. E. Dmitrienko, Sov. Sci. Rev., Sect. A **13**, 1 (1989).
[20] S. Chandrasekhar, *Liquid Crystals* (Cambridge University Press, London, 1992).
[21] H. de Vries, Acta Crystallogr. **4**, 219 (1951).
[22] O. Parodi, J. Phys. (Paris), Colloq. **36**, C1-22 (1975).
[23] D.-H. Chung, MS thesis, Tokyo Institute of Technology, Japan, 2000.
[24] R. Dreher, G. Meier, and A. Saupe, Mol. Cryst. Liq. Cryst. **13**, 17 (1971).
[25] H. Takezoe, Y. Ouchi, M. Hara, A. Fukuda, and E. Kuze, Jpn. J. Appl. Phys., Part 1 **22**, 1080 (1983).